# Investigating the Stability of the Phase Field Solution of Equilibrium Droplet Configurations by Eigenvalues and Eigenvectors

Felix Diewald[a,*], Charlotte Kuhn[b], Michaela Heier[c], Kai Langenbach[c,d], Martin Horsch[c,e], Hans Hasse[c], Ralf Müller[a]

[a]*Institute of Applied Mechanics, University of Kaiserslautern, 67653 Kaiserslautern, Germany*
[b]*Computational Mechanics, University of Kaiserslautern, 67653 Kaiserslautern, Germany*
[c]*Laboratory of Engineering Thermodynamics, University of Kaiserslautern, 67653 Kaiserslautern, Germany*
[d]*Department of Chemical and Biomolecular Engineering, Rice University, 6100 Main St., Abercrombie Laboratory, Houston, TX 77005-1827, USA*
[e]*Department of Chemical Engineering, Indian Institute of Technology Kanpur, Kalyanpur, UP-208016, India*

## Abstract

Phase field models have recently been used to investigate the physical behavior of droplets in static as well as dynamic situations. As those models are often driven by an Allen-Cahn evolution equation, their stationary solution is given by the first order optimality condition of an energy functional. This includes the possibility of computing saddle points and maxima rather than minima of the energy functional. The present work shows the post-processing of eigenvalues and eigenvectors of the system matrix of the phase field model in order to investigate the stability of equilibrium droplet configurations. This post-processing can easily be ported to other evolution equations. The underlying phase field model is described and the resulting discrete finite element eigenvalue problem is stated. The investigation of eigenvalues and eigenvectors is illustrated by examples.

*Keywords:* droplets, stability, eigenvalues, eigenvectors, phase field

## 1. Introduction

Understanding how droplets interact with each other as well as the ability to predict wetting phenomena is highly important in a variety of applications, e.g. pyrometallurgical processes [1] or inkjet printing [2]. Phase field simulations in which the presence of a phase is described by a continuous order parameter are capable of gaining this knowledge not only for a two-phase system but also for systems with multiple phases [3, 4, 5].

Depending on the case of application, some phase field models examine the static equilibrium [3] of droplets while others investigate the dynamics of (possibly) multi-component fluid flows [2]. Phase field models offer a straightforward way to consider dynamic as well as static wetting scenarios on a variety of surface geometries. Especially in the case of microstructured surface wetting a profound knowledge of the static equilibrium wetting state of droplets is relevant and can serve as a starting point for a deeper understanding of the underlying effects. Regarding dynamic wetting of microstructured surfaces makes it harder to distinguish between the different effects due to a greater number of parameters.

The fact that there is often a large difference between the initialization state of the phase field calculation and the final solution brings the necessity of using an evolution equation in order to gradually relax the phase field towards the static solution. Most commonly, an Allen-Cahn [6, 3, 7] or Cahn-Hilliard (see for instance [2] and the references therein) type evolution equation is chosen.

In order to give the phase field models a physical relevance, molecular simulations can provide a link to the required input parameters for the phase field model and interaction potentials [8]. Phase field studies that obtain their input parameters from molecular simulations can, for instance, be found in [8, 9, 10, 11]. Crucial input parameters for phase field models investigating droplet behavior, like the contact angle or the width of the transition zone between the liquid and the gas phase, could, for example, be derived from [12].

When using a phase field model to compute the static equilibrium configuration of a droplet that is in contact with a solid surface the solution is given by the first order optimality condition of an energy functional. As this can lead to a computation of saddle points and maxima rather than minima of the energy functional, a closer investigation of the obtained solution becomes necessary in order to determine the stability of the solution and if a minimum energy configuration is attained. While much work has been done on the stability analysis of droplet on a variety of different substrates, see e.g. [13, 14, 15, 16, 17, 18, 19, 20, 21, 22], the investigation of the static solution state of a phase field model in order to determine the character of the obtained solution needs (to the best of the authors'

---

*Corresponding author
Email address:* `fdiewald@rhrk.uni-kl.de` (Felix Diewald)

knowledge) yet to be done and is the main purpose of the present work.

The basic framework of computing the solution of a phase field model by solving the first order optimality condition of an energy functional is commonly used in a variety of different phase field models. Therefore, the presented post-processing can easily be adapted to a wide range of phase field models and is not limited to the specific case presented in this paper.

The following sections will first give an introduction to the underlying phase field model. Subsequently, an investigation of the eigenvalues and eigenvectors of the system matrix and thereby of the stability of droplet shapes is undertaken. In order to illustrate the stability analysis three examples are presented.

## 2. Phase field model

The present work incorporates a phase field model for a two-phase droplet system (liquid/gas) that is capable of regarding the contact angle between the liquid and a solid surface as well as preserving a specified droplet volume. Since the static solution of small-scale droplets is considered, the influence of gravity is neglected. After a description of the phase field model some details of the numerical implementation are given and the considered eigenproblem is formulated.

### 2.1. Model description

Based upon a continuous order parameter $\varphi(\boldsymbol{x}, t)$ that indicates whether the gas or the liquid phase is present at a certain location

$$\varphi = \begin{cases} 0, & \text{for gas} \\ 1, & \text{for liquid} \end{cases}, \qquad (1)$$

the free energy $F$ is defined as

$$
F = \int_\Omega \left[ 12 \frac{\gamma_{GL}}{\kappa} f(\varphi) + \frac{3}{4} \gamma_{GL} \kappa |\nabla \varphi|^2 \right] \mathrm{d}V
$$
$$
+ \lambda \left( \int_\Omega h(\varphi) \mathrm{d}V - V_0 \right) \qquad (2)
$$
$$
+ \int_{\partial \Omega_s} [h(\varphi) \gamma_{SL} + (1 - h(\varphi)) \gamma_{SG}] \, \mathrm{d}A .
$$

Here, $\Omega$ is the domain in which the gas and the liquid phase exist and $\partial \Omega_s$ denotes the part of the boundary where $\Omega$ is bounded by a solid surface. In the following, $F$ is simply referred to as energy. The first contribution to $F$ includes the separation and gradient terms which are well known for phase field models. The surface tension between the gas and the liquid phase is given by $\gamma_{GL}$ and $f(\varphi)$ is a classical double well potential

$$f(\varphi) = \varphi^2 (1 - \varphi)^2 . \qquad (3)$$

The separation and gradient terms are weighted in such a way that the width of the transition zone between gas

and liquid can be adjusted by $\kappa$. In order to give $\kappa$ a physical meaning it can be set to a value that represents the width of the density gradient between liquid and gas (approximately 1nm). As mentioned this width can be obtained from molecular simulations. However, since the width of the transition zone between gas and liquid needs to be resolved by an adequate number of finite elements, simulations that are not done on a molecular scale require a larger choice of $\kappa$ in order to limit the numerical cost. For an interpretation of the parameters in phase field simulations, see e.g. [23]. A deeper discussion of the width of the transition zone and the so called sharp-interface limit beyond which the phase field results do not depend on the width of the transition zone can for instance be found in [24] or [25].

Solely minimizing the energy contributed by the surface tension $\gamma_{GL}$ would inevitably cause the drop to shrink and vanish. Therefore, an additional volume constraint has to be added in order to prescribe the liquid volume $V_l$. Ideas to enforce a volume constraint within a phase field model are presented in [6] and [4]. In the present work we choose a Lagrange multiplier $\lambda$ to incorporate the volume constraint (second contribution to (2)). In comparison to a penalty term this adds one global degree of freedom $\lambda$ which only marginally rises the numerical cost for the finite element implementation. During the simulation, the liquid volume $V_l = \int_\Omega h(\varphi) \mathrm{d}V$ is conserved with the target volume $V_0$ without the need of computing and updating an intermediate solution. Therefore, the volume constraint does not contribute to the free energy of the domain. The value of $\lambda$ is equivalent to the difference between the pressure inside and outside of a droplet which can also be obtained analytically by the Young-Laplace equation for spherical droplets [26].

The third contribution to (2) adds the energy contributions of the surface tension between the solid surface and the liquid $\gamma_{SL}$ as well as the surface tension between the solid surface and the gas $\gamma_{SG}$ and allows for an adjustment of the contact angle $\Theta$ between a droplet and a solid surface [3]. With these energy contributions the natural boundary conditions read

$$\frac{3}{2} \gamma_{GL} \kappa \nabla \varphi \cdot \overrightarrow{n} + h'(\varphi)(\gamma_{SL} - \gamma_{SG}) = 0 , \qquad (4)$$

for the part of the boundary where $\Omega$ is bounded by a solid surface $\partial \Omega_s$ and

$$\nabla \varphi \cdot \overrightarrow{n} = 0 , \qquad (5)$$

for the remaining boundary of $\Omega$. Here, $\overrightarrow{n}$ is the outer normal to the boundary. Young's equation for the contact angle

$$\cos \Theta = \frac{\gamma_{SG} - \gamma_{SL}}{\gamma_{GL}} \qquad (6)$$

is not explicitly prescribed. However, it can be shown that boundary condition (4) leads to Young's equation. For more details the reader is referred to [27].

2

For numerical reasons (smoothness and stability) the interpolation function [28]

$$h(\varphi) = \varphi^3(6\varphi^2 - 15\varphi + 10) \qquad (7)$$

is introduced in (2). For both, the volume constraint as well as the energy contribution from the contact with the solid, this smooth function brings the advantage that $h'(0) = 0$ and $h'(1) = 0$ while satisfying $h(0) = 1$ and $h(1) = 1$.

Cahn-Hilliard type approaches have a stiff numerical behavior due to the fourth order spatial derivatives and (low order) bilinear elements cannot be applied [29]. For their implementation in the FE context techniques like mixed finite element methods, coupled equations, interpolation functions that have a high degree of continuity, or a discontinuous Galerkin method are required [30]. Without claiming completeness we cite [30, 31, 32, 29]. In the context of explicit finite differences the Cahn-Hilliard type approach requires small time steps thus the identification of equilibrium states is very cumbersome. To bypass these drawbacks an evolution equation of Allen-Cahn [33] type is chosen for the presented FE model as it allows for a simpler and therefore resource efficient implementation [7] and has proven to be useful for the simulation of droplets [3, 6, 7]. Although the Allen-Cahn evolution equation might follow a different kinetic path to find the static equilibrium state of a droplet it will reach the same stationary solution as the Cahn-Hilliard approach [3]. In certain scenarios, the Allen-Cahn evolution equation can also be used to investigate time dependent droplet behavior. In a recent work regarding drop evaporation [34] the mobility parameter is experimentally fit to substitute the diffusion coefficient. Unlike the Cahn-Hilliard type approach the Allen-Cahn type evolution equation does not by itself conserve the volume of the order parameter [7]. However, since (2) includes a volume constraint this is no drawback. Firstly,

$$\dot{\varphi} = -M\frac{\delta_\varphi F}{\delta\varphi} \quad \text{and} \quad \delta_\lambda F = 0 \qquad (8)$$

are solved for a number of computational time steps in order to shorten the "distance" to the stationary solution. Note that in this context the sequence of computational time steps should not bee seen as the dynamic behavior of the droplet but as a numerical relaxation towards the stationary solution. In (8), $\delta_b A$ is the first variation of $A$ with respect to $b$ and $M$ the mobility. In the vicinity of the stationary solution

$$\int_\Omega 0.5\left(\frac{\dot{\varphi}}{M}\right)^2 \mathrm{d}V \leq \mathrm{tol}\,, \qquad (9)$$

the evolution equation is replaced by the quasi-static limit condition

$$\delta_\varphi F = 0 \quad \text{and} \quad \delta_\lambda F = 0\,. \qquad (10)$$

Solving (10) includes the possibility of computing saddle points and maxima rather than minima of the energy.

The use of an evolution equation as (8) can lead to configurations that represent a saddle point, maximum or lie within an unstable region of the energy landscape. This can happen if the computation is started with an initialization that is close to a saddle point or maxima.

If (by chance) the computation is started with an initialization corresponding to a saddle point or maximum, the evolution equation (8) would never lead away from that saddle point or maximum.

If the initialization is just close to a saddle point or maximum of the free energy, the evolution equation (8) would lead away from that saddle point or maximum towards a local minimum. However, this evolution would be very slow in the vicinity of the saddle point or maximum as $\delta F$ would be small in this region. It is always cumbersome to determine when a solution is reached by the evolution equation. Therefore, it is suggestive to use a velocity norm (9) to determine if the evolution has brought the phase field sufficiently close to the actual solution. The fact that this velocity norm would be very small in the vicinity of a saddle point or maximum would promote the conclusion that a solution was found and the evolution can be stopped. If (10) is used afterwards the phase field would eventually converge to a configuration representing a saddle point or maximum. But even if (10) is not used the configuration would still be close to the saddle point or maximum. Therefore, the found configuration would potentially lie within an unstable region of the energy landscape and would not be close to a local minimum. The presented post-processing can reveal the fact that the found configuration (which would be viewed as a solution) is in fact not a solution. In practice, the presented post-processing does therefore not only become important in the rare event of starting with an initialization exactly representing a saddle point or maximum but also when starting with an initialization that lies within the vicinity of a saddle point or maximum.

In other applications of phase field models (especially for coupled problems) the presented post-processing can gain additional relevance. In the case of phase field models for fracture the energy landscape can change due to outer loads. This can turn a former local minimum into a saddle point or maximum. The presented procedure could be applied to determine if this is the case.

As (10) is not dependent on the choice of evolution equation that is used to shorten the "distance" to the stationary solution, the presented post-processing can easily be adapted to models utilizing a different evolution equation.

### 2.2. Residuum and linearization

Newton's method is used to fulfill (8) and (10) respectively. Following common finite element procedure the deviations of the current state of the regarded domain from (8) or (10) will be referred to as residuals. Expressions for the residuals and linearizations of the residuals are given in the present section.

Using (8) the residual with respect to $\varphi$ (referring to the left equation in (8)) reads

$$R_\varphi = \int_\Omega \left[ 12 \frac{\gamma_{GL}}{\kappa} f'(\varphi)\delta\varphi + \frac{3}{2}\gamma_{GL}\kappa\nabla\varphi\nabla(\delta\varphi) \right] \mathrm{d}V$$
$$+ \lambda \int_\Omega h'(\varphi)\delta\varphi \mathrm{d}V + \int_\Omega \frac{\dot\varphi}{M}\delta\varphi \mathrm{d}V \qquad (11)$$
$$+ \int_{\partial\Omega_s} h'(\varphi)(\gamma_{SL} - \gamma_{SG})\delta\varphi \mathrm{d}A \,.$$

Note that the energy contribution from the surface is influenced by the difference between $\gamma_{SL}$ and $\gamma_{SG}$ only and not by their absolute values, which is in good agreement with Young's equation. The residual with respect to the global degree of freedom $\lambda$ (referring to the right equation in (8)) is given by

$$R_\lambda = \left( \int_\Omega h(\varphi)\mathrm{d}V - V_0 \right)\delta\lambda \,. \qquad (12)$$

With $D_b(A)\Delta b$ as the linearization of $A$ with respect to $b$ the linearizations of (11) and (12) can be written as

$$K_{\varphi\varphi} = D_\varphi(R_\varphi)\Delta\varphi + D_{\dot\varphi}(R_\varphi)\Delta\dot\varphi$$
$$= \int_\Omega \left[ 12\frac{\gamma_{GL}}{\kappa} f''(\varphi)\delta\varphi\Delta\varphi \right.$$
$$\left. + \frac{3}{2}\gamma_{GL}\kappa\nabla(\delta\varphi)\nabla(\Delta\varphi) \right]\mathrm{d}V \qquad (13)$$
$$+ \int_\Omega \lambda h''(\varphi)\delta\varphi\Delta\varphi \mathrm{d}V + \int_\Omega \frac{1}{M}\delta\varphi\Delta\dot\varphi \mathrm{d}V$$
$$+ \int_{\partial\Omega_s} h''(\varphi)(\gamma_{SL} - \gamma_{SG})\delta\varphi\Delta\varphi \mathrm{d}A \,,$$

$$K_{\varphi\lambda} = D_\lambda(R_\varphi)\Delta\lambda = \int_\Omega h'(\varphi)\delta\varphi\Delta\lambda \mathrm{d}V \,, \qquad (14)$$

$$K_{\lambda\varphi} = D_\varphi(R_\lambda)\Delta\varphi = \int_\Omega h'(\varphi)\mathrm{d}V\delta\lambda\Delta\varphi \,, \qquad (15)$$

$$K_{\lambda\lambda} = D_\lambda(R_\lambda)\Delta\lambda = 0 \,. \qquad (16)$$

*2.3. Discretization and eigenproblem*

The finite element discretization of the degree of freedom $\varphi$ on element level reads

$$\varphi^e = \overline{N}\overline{\varphi} = \begin{bmatrix} N_1 & N_2 & ... & N_n \end{bmatrix} \begin{bmatrix} \varphi_1 \\ \varphi_2 \\ ... \\ \varphi_n \end{bmatrix}, \qquad (17)$$

and for $\lambda$ on the global level

$$\lambda^g = \overline{N_\lambda}\,\overline{\lambda}. \qquad (18)$$

Here, $N_i$ $(i = 1, 2, ..., n)$ are the shape functions for a number of $n$ nodes on every element and $\varphi_i$ the respective nodal values. Note that $\overline{N_\lambda} = 1$ as it belongs to the global degree of freedom $\lambda$ which is located on the entire domain and therefore not associated with a distinct node of the mesh $(\overline{\lambda} = \lambda)$. As described in our recent work [35] 4-node and 2-node elements are used in the two-dimensional case for the energy contributions of the region and the surface respectively. In the vicinity of the solution, where (10) is solved instead of (8), Newton's method leads to the global system

$$\begin{bmatrix} \overline{\delta\varphi}^T \\ \overline{\delta\lambda}^T \end{bmatrix} \left( \underbrace{\begin{bmatrix} \overline{K_{\varphi\varphi}} & \overline{K_{\varphi\lambda}} \\ \overline{K_{\lambda\varphi}} & 0 \end{bmatrix}}_{\boldsymbol{K}} \begin{bmatrix} \overline{\Delta\varphi} \\ \overline{\Delta\lambda} \end{bmatrix} = \begin{bmatrix} \overline{R_\varphi} \\ \overline{R_\lambda} \end{bmatrix} \right),$$
$$(19)$$

with

$$\overline{R_\varphi} = \int_\Omega \left[ 12\frac{\gamma_{GL}}{\kappa} f'(\varphi)\overline{N}^T + \frac{3}{2}\gamma_{GL}\kappa\nabla\varphi\overline{B}^T \right.$$
$$\left. + \lambda h'(\varphi)\overline{N}^T \right]\mathrm{d}V \qquad (20)$$
$$+ \int_{\partial\Omega_s} h'(\varphi)(\gamma_{SL} - \gamma_{SG})\overline{N}^T\mathrm{d}A \,,$$

$$\overline{R_\lambda} = \left( \int_\Omega h(\varphi)\mathrm{d}V - V_0 \right)\overline{N_\lambda}^T \,, \qquad (21)$$

$$\overline{K_{\varphi\varphi}} = \int_\Omega \left[ 12\frac{\gamma_{GL}}{\kappa} f''(\varphi)\overline{N}^T\overline{N} + \frac{3}{2}\gamma_{GL}\kappa\overline{B}^T\overline{B} \right.$$
$$\left. + \lambda h''(\varphi)\overline{N}^T\overline{N} \right]\mathrm{d}V \qquad (22)$$
$$+ \int_{\partial\Omega_s} h''(\varphi)(\gamma_{SL} - \gamma_{SG})\overline{N}^T\overline{N}\mathrm{d}A \,,$$

$$\overline{K_{\varphi\lambda}} = \int_\Omega h'(\varphi)\overline{N}^T\overline{N_\lambda}\mathrm{d}V \,, \qquad (23)$$

$$\overline{K_{\lambda\varphi}} = \overline{K_{\varphi\lambda}}^T \,. \qquad (24)$$

Here, $\boldsymbol{K}$ is the global tangent matrix of the system and $\overline{B}$ contains the spatial derivatives of the shape functions. Once (10) is solved within tolerance the eigenproblem studied in the present work reads

$$(\boldsymbol{K}_{\mathrm{sol}} - \Lambda\boldsymbol{1})\boldsymbol{v} = \boldsymbol{0} \,. \qquad (25)$$

With $\boldsymbol{K}_{\mathrm{sol}}$ being the global tangent matrix of the solution state of (10). Nontrivial solutions of (25) yield the eigenvalues $\Lambda$ and the normalized eigenvectors $\boldsymbol{v}$.

The eigenvector $\boldsymbol{v}$ represents a perturbation from the solution state of the degrees of freedom $\begin{bmatrix} \overline{\varphi} & \overline{\lambda} \end{bmatrix}^T$. A positive eigenvalue $\Lambda$ connotes that the change in the residuals $\begin{bmatrix} \overline{R_\varphi} & \overline{R_\lambda} \end{bmatrix}^T$ that is caused by this disturbance has the same sign as the disturbance $\boldsymbol{v}$ itself, which indicates that the solution lies within a convex (stable) region of the free energy of the entire system. Analogously a negative eigenvalue $\Lambda$ reveals that the found solution is not stable. A subspace iteration is used to extract the lowest $n_e$ eigenpairs.

In [36] the authors use a similar approach in order to evaluate the modes of initial droplet growth for droplet

Table 1: Input parameters (and analytic contact angle) for two-dimensional (a) droplets without and with surface contact and (b) droplets placed on pedestal

| parameter | values (a) | values (b) |
|---|---|---|
| $\gamma_{GL}$ | 1.000 | 1.000 |
| $\gamma_{SL}$ | 1.000 | [0.357,1.174] |
| $\gamma_{SG}$ | 1.000 | 1.000 |
| $\Theta$ | 90° | [50°,100°] |
| $\kappa$ | 1.0 | 1.0 |
| $\kappa/h_c$ | 3.2 | - |
| $\kappa/h_f$ | 6.4 | - |
| $\kappa/h_p$ | - | 12.8 |
| $M$ | - | 100.0 |
| $\Delta t$ | - | 0.005 |

nucleation. Considering a solution profile for a nucleating droplet, they expand the free energy of their system to second order and examine the change of the free energy for a perturbation of the order parameter away from the solution state. To do so, the authors investigate the eigenvalues and eigenvectors of the second order term of their energy expansion (compare to $\boldsymbol{K}_{\mathrm{sol}}$). They derive a single negative eigenvalue whose corresponding eigenvector describes how the droplet will initially grow. While the methodology of [36] is similar to the one presented in this work, their application is quite different. In [36] the authors use the investigation of eigenvalues and eigenvectors in order to predict how a nucleating droplet will grow. The present work uses the investigation of eigenvalues and eigenvectors of the system matrix in order to determine whether a state of a phase field model that fulfills the first order optimality condition of the energy function is a true solution or not. The application presented in this work is not limited to droplets and can be used for other phase field models as well.

## 3. Numerical examples

In the following three different two-dimensional scenarios are examined. First a droplet that is not in contact with a surface and second a droplet that is in contact with a solid surface is considered. Thereafter, an analysis of two different configurations of a droplet on a pedestal is presented. The procedure for all three examples is the following:

1. relax the phase field towards the stationary solution using (8)
2. compute the stationary solution using (10)
3. investigate the eigenvalues and eigenvectors of the global tangent matrix $\boldsymbol{K}_{\mathrm{sol}}$ using (25)

An equidistant mesh was used for each of the computations. Note that all input parameters for the numerical computations are dimensionless. As the present work is pursuing the investigation of the eigenvalues and the eigenvectors for different scenarios, this is no drawback.

### 3.1. Droplet without surface contact

The considered domain for the two-dimensional droplet without surface contact is a square area. The computation is performed on a coarse mesh with the element edge length $h_c$ and $\kappa/h_c = 3.2$ as well as on a fine mesh with the element edge length $h_f$ and $\kappa/h_f = 6.4$. The input parameters are given in Table 1(a). The minimum energy configuration was directly computed without the use of the evolution equation. After the computation of the solution the eigenvalues and eigenvectors are calculated. Fig. 2 shows the eight eigenvalues with the smallest absolute values for the computation with (a) the coarse and (b) the fine mesh.

For each computation, the eigenvalues come in pairs of similar size. The most substantial difference between the eigenvalues of the computation with the coarse and the fine mesh is found in the first two eigenvalues. For the refined mesh, they are closer to zero by five orders of magnitude without the other eigenvalues changing that significantly. Since a translation of the droplet was not confined and would not lead to an immediate energy change, it is obvious that the first two eigenvalues which are close to zero belong to eigenvectors that describe a purely translational movement of the droplet. Fig. 1 ($i = 1, 2$) underlines this fact which is in accordance with [36]. The figure shows contour plots of the sum $\boldsymbol{v}_i + \boldsymbol{\varphi}$ with $\boldsymbol{v}_i$ being the eigenvector that belongs to the $i^{\text{th}}$ eigenvalue and $\boldsymbol{\varphi}$ being the solution state of the discretized phase field. The white circles represent the $\varphi = 0.5$ isoline of the phase field. The depicted contour plots belong to the computation with the coarse mesh and do not show the entire domain. The coarse mesh is close to being too coarse to resolve the transition region between the gas and the liquid phase. However, since a scaling of the resulting eigenvectors does not scale the drop deformation, the coarse computation was chosen for the contour plots as it emphasizes the droplet movement or deformation. Nonetheless, the computation with the finer mesh emphasizes the fact that there is no energy change for a purely translational movement of the droplet.

The contour plots for $i = 3$ and $i = 4$ show the first-degree droplet deformations. The second-degree droplet deformations are addressed by the contour plots for $i = 5$ and $i = 6$. Note that a rise of the degree of deformation which is equivalent to an increase of the frequencies in the shape change along the perimeter of the droplet is accompanied by a rise of the eigenvalues. Furthermore, the deformations that belong to the same degree of deformation and do only differ by a rotation of the deformation correspond to eigenvalues of almost equal size. The fact that all these deformations belong to positive eigenvalues indicates that a droplet that is deformed in such a way will restore its circular shape in order to minimize the energy.

### 3.2. Droplet with surface contact

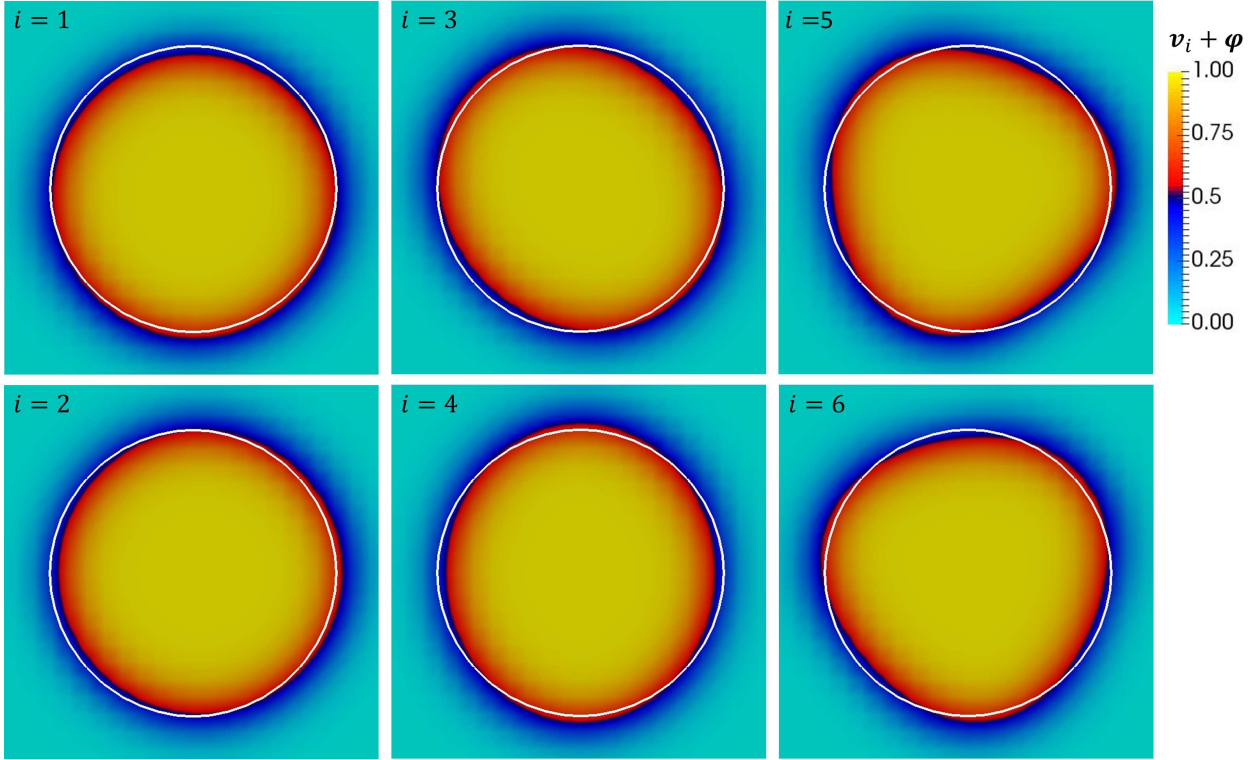The second scenario represents a variation of the first example. Without changing the input parameters, the

Figure 1: Contour plots of $\boldsymbol{v}_i + \boldsymbol{\varphi}$ for two-dimensional droplet without surface contact for the first six eigenvectors, coarse mesh
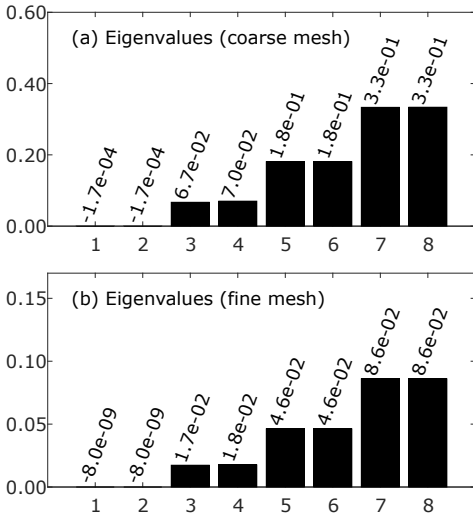


Figure 2: First eight eigenvalues (sorted by smallest absolute values) of two-dimensional droplet without surface contact, (a) coarse mesh, (b) fine mesh

droplet is placed on a solid surface. The input parameters are therefore also given in Table 1(a). Fig. 4 shows the eight eigenvalues with the smallest absolute values for the computation with (a) the coarse and (b) the fine mesh.

It is evident that the eigenvalues do not come in pairs of similar size as it was the case for the droplet without surface contact. The most substantial difference between the computation with the coarse and with the fine mesh is only found in the first eigenvalue. Nevertheless, the magnitudes of the differences between the eigenvalues of the computation with the coarse and the computation with the fine mesh are the same as it was the case for the droplet without surface contact. Fig. 3 explains these results. As before, the figure shows contour plots of the sum $\boldsymbol{v}_i + \boldsymbol{\varphi}$ for the computation with the coarse mesh with the white line representing the $\varphi = 0.5$ isoline of the phase field. The plots do not show the entire domain. As expected the first eigenvalue belongs to a horizontal translation of the droplet. As the solid surface is confining a free translational movement in vertical direction such a movement is not found within the first eight eigenvalues.

The first-degree and second-degree droplet deformations are shown by the contour plots for $i = 2$ and $i = 3$. Unlike in the scenario of the droplet without surface contact there is no rotated deformation of the same degree. This can also be explained by the contact with the solid surface. Comparing the eigenvalues of the corresponding deformations of the droplet without and the droplet with surface contact reveals that they are of similar size. This
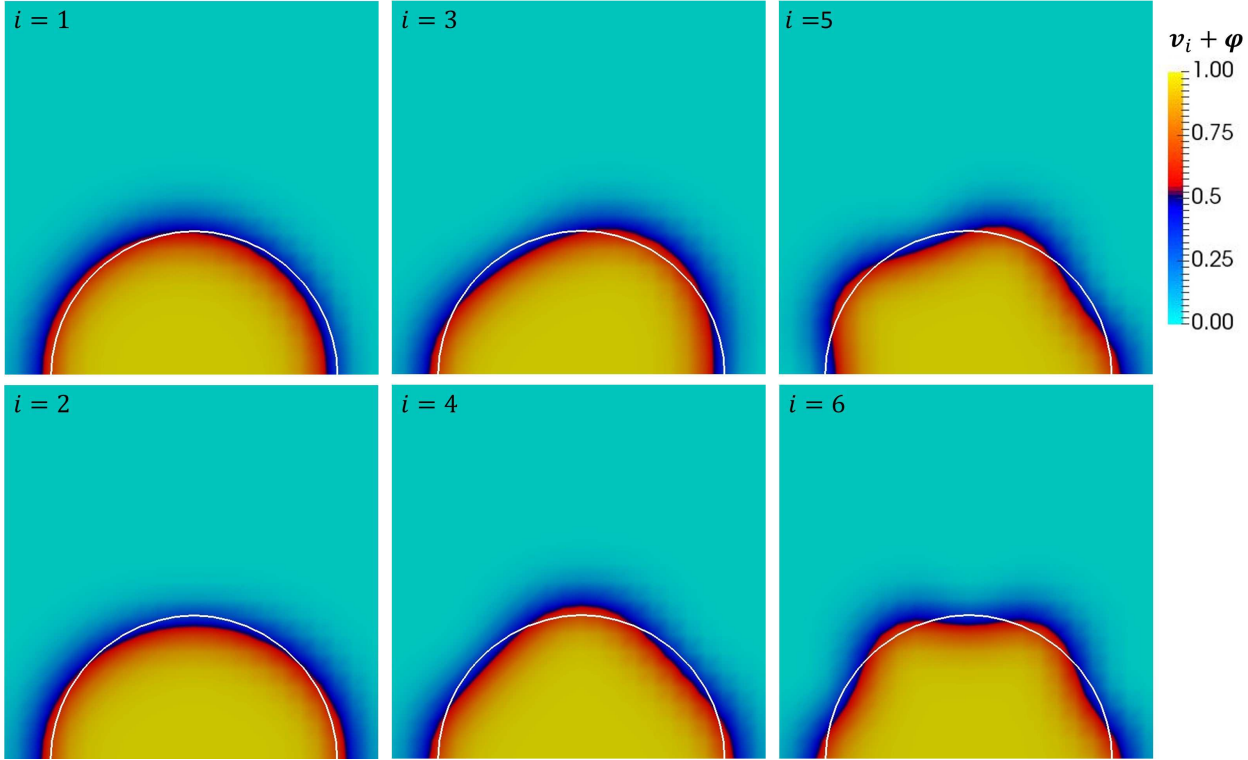
Figure 3: Contour plots of $v_i + \varphi$ for two-dimensional droplet with surface contact for the first six eigenvectors, coarse mesh
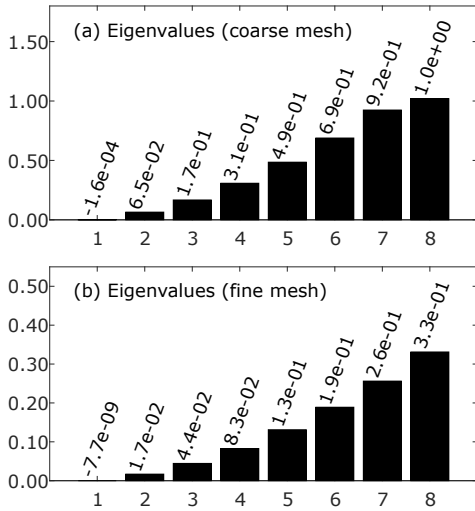


Figure 4: First eight eigenvalues (sorted by smallest absolute values) of two-dimensional droplet with surface contact, (a) coarse mesh, (b) fine mesh

holds true for the computation with the coarse mesh as well as for the computation with the fine mesh. Again, a rise of the degree of droplet deformation is accompanied by a rise of the corresponding eigenvalues. This becomes even more evident when looking at the contour plots for $i = 4, 5, 6$. The eigenvectors define shapes of droplets that are similar to those of vibrating droplets, see for example [37].

### 3.3. Droplet on pedestal

The next scenario under consideration is a droplet placed on a pedestal. As Fig. 5(a+b) show, there exist at least two different solution configurations depending on how the computation is initialized. The configuration in which the droplet is placed on the edge of the pedestal, cf. Fig. 5(a), was realized by using an initialization with a droplet that is centered directly on the edge of the pedestal and therefore corresponding to the stationary solution (Fig. 5(a)). The configuration in which the droplet is placed on top of the pedestal, cf. Fig. 5(b), was realized by initializing the computation with a droplet that is located a little off-center thus breaking the symmetry and causing the droplet to travel on top of the pedestal during the phase field evolution. The plots do not show the entire domain and the input parameters are given in Table 1(b). Fig. 6 shows a comparison of the energy $F$ for the droplet on the edge and the droplet on top of the pedestal for different contact angles $\Theta$. For all considered contact angles $\Theta$, the droplet on the edge of the pedestal has a hig-
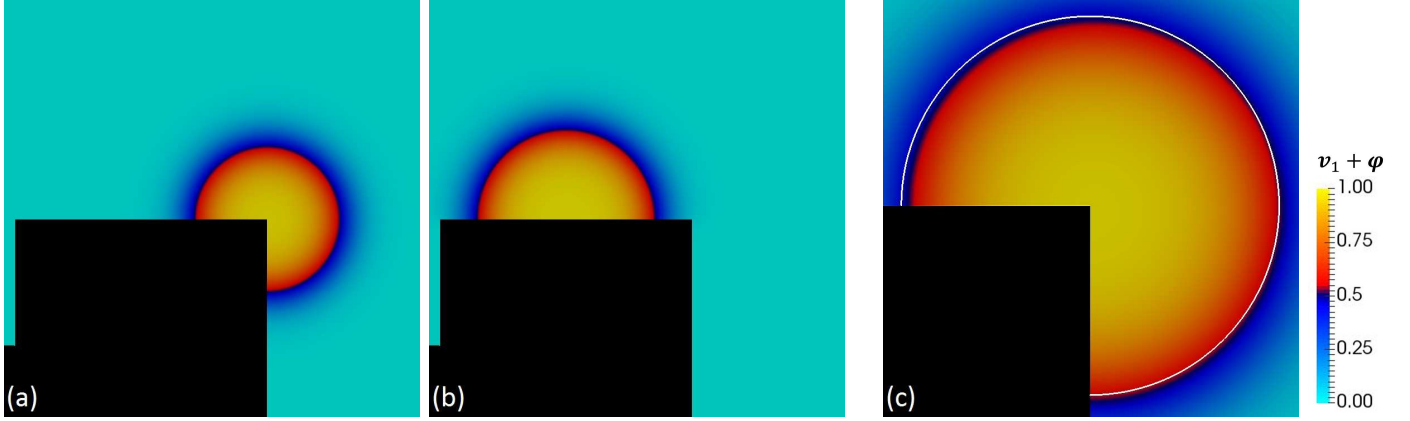
Figure 5: Two possible solutions for two-dimensional droplet placed on a pedestal (black area): (a) computation initialized with droplet centered directly on the edge of pedestal, (b) computation initialized with droplet located a little off-center. (c) Contour plot of $\boldsymbol{v}_1 + \boldsymbol{\varphi}$ for two-dimensional droplet on the edge of a pedestal ($\Theta = 90°$)
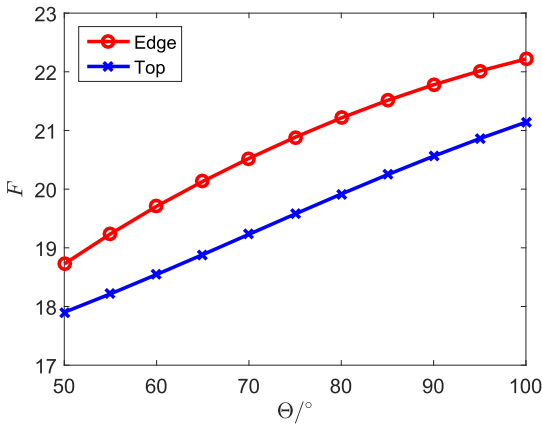


Figure 6: Energy of two-dimensional droplets on the edge and on top of a pedestal for different contact angles $\Theta$
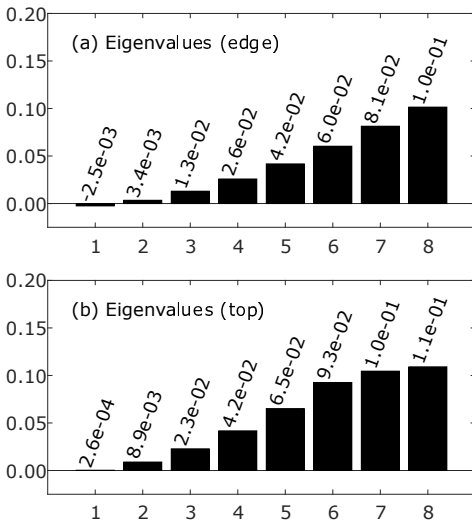


Figure 7: First eight eigenvalues (sorted by smallest absolute values) of two-dimensional droplets (a) on the edge and (b) on top of a pedestal ($\Theta = 90°$)

her energy than the droplet on top of the pedestal. From this it is clear that the configuration with the droplet on the edge of the pedestal cannot represent a global energy minimum. The question that arises from this fact is whether it represents a local minimum, a saddle point, or a maximum. Or phrased differently, whether it is a metastable or unstable configuration. The computation of the eigenvalues of the two configurations for $\Theta = 90°$ reveals the results shown in Fig. 7. The first eigenvalue of the droplet on the edge of the pedestal is negative (Fig. 7(a)). Fig 5(c) shows a contour plot of the sum $\boldsymbol{v}_1 + \boldsymbol{\varphi}$. Again, the white line is the $\varphi = 0.5$ isoline of the phase field. It becomes clear that the negative eigenvalue belongs to a droplet movement away from the center of the edge of the pedestal. This implies that the configuration with the droplet on the edge of the pedestal is not stable. Considering how the computation was initialized the configuration with the drop on the edge of the pedestal is not strictly unphysical. However, the negative eigenvalue states that this configuration can only be reached in an undisturbed environment, which by itself would represent an too ideal assumption. Even the smallest imperfection of the droplet would cause it to move away from the edge. This fact would not have been revealed by the phase field model without the presented post-processing of eigenvalues and eigenvectors. Although a very fine mesh was used (element edge length $h_p$ and $\kappa/h_p = 12.8$), the first eigenvalue of the droplet on top of the pedestal (Fig. 7(b)) is further away from zero (five orders of magnitude) as it was the case for the droplet without surface contact (Fig. 2(b)). This can be caused by a weak confinement of the translational movement and can be explained by the fact that the droplet is still influenced by the two edges to its right and left (Fig. 5(b)). Therefore, the droplet is traveling to the center of the upper surface of the pedestal although the computation was initialized with a droplet located a just bit off-center from the edge of the pedestal.

8

## 4. Conclusion

It was shown that, in the case of phase field computations regarding droplets, the investigation of the eigenvalues and the eigenvectors of the system matrix leads to a better understanding of the energy changes for simple droplet deformations and can furthermore be a useful tool in order to determine the stability of a solution. Whenever a solution is obtained by the first order optimality condition of an energy functional $\delta F = 0$ (as is usually the case for phase field simulations) one might compute minimum energy configurations but cannot directly rule out the possibility of obtaining a saddle point or a maximum of the energy functional. In all these cases, the presented investigation of eigenvalues and eigenvectors could be applied in order to investigate the character of the obtained solution. Especially by visualizing the impact of the eigenvectors on the phase field variable it is not only possible to determine whether a saddle point or maximum instead of a minimum of the energy functional was found but also in which direction the phase field would need to evolve in order to move away from that saddle point or maximum. This suggests to use the presented post-processing not only for the present droplet case but also for other phase field models.

[1] I. Bellemans, N. Moelans, K. Verbeken, Phase field modelling of the attachment of metallic droplets to solid particles in liquid slags: Influence of interfacial energies and slag supersaturation, Computational Materials Science 108 (2015) 348–357. doi:10.1016/j.commatsci.2015.03.019.

[2] J. S. Kim, Phase-Field Models for Multi-Component Fluid Flows, Communications in Computational Physics 12 (2012) 613–661. doi:10.4208/cicp.301110.040811a.

[3] M. Ben Said, M. Selzer, B. Nestler, D. Braun, C. Greiner, H. Garcke, A phase-field approach for wetting phenomena of multiphase droplets on solid surfaces, Langmuir 30 (14) (2014) 4033–4039. doi:10.1021/la500312q.

[4] B. Nestler, F. Wendler, M. Selzer, B. Stinner, H. Garcke, Phase-field model for multiphase systems with preserved volume fractions, Physical Review E 78 (1) (2008) 011604. doi:10.1103/PhysRevE.78.011604.

[5] H. Garcke, B. Nestler, B. Stoth, A MultiPhase Field Concept: Numerical Simulations of Moving Phase Boundaries and Multiple Junctions, SIAM Journal on Applied Mathematics 60 (1) (1999) 295–315. doi:10.1137/S0036139998334895.

[6] H. Garcke, B. Nestler, B. Stinner, F. Wendler, ALLEN–CAHN SYSTEMS WITH VOLUME CONSTRAINTS, Mathematical Models and Methods in Applied Sciences 18 (8) (2008) 1347–1381. doi:10.1142/S0218202508003066.

[7] X. Yang, J. J. Feng, C. Liu, J. Shen, Numerical simulations of jet pinching-off and drop formation using an energetic variational phase-field method, Journal of Computational Physics 218 (1) (2006) 417–428. doi:10.1016/j.jcp.2006.02.021.

[8] M. Berghoff, M. Selzer, B. Nestler, Phase-Field Simulations at the Atomic Scale in Comparison to Molecular Dynamics, Scientific World Journal 2013 (4) (2013) 1–8. doi:10.1155/2013/564272.

[9] J. Bragard, A. Karma, Y. H. Lee, M. Plapp, Linking Phase-Field and Atomistic Simulations to Model Dendritic Solidification in Highly Undercooled Melts, Interface Science 10 (2/3) (2002) 121–136. doi:10.1023/A:1015815928191.

[10] B. Nestler, M. Selzer, D. Danilov, Phase-field simulations of nuclei and early stage solidification microstructures, Journal of Physics: Condensed Matter 21 (46) (2009) 464107. doi:10.1088/0953-8984/21/46/464107.

[11] G. Tegze, T. Pusztai, G. Toth, L. Granasy, A. Svandal, T. Buanes, T. Kuznetsova, B. Kvamme, Multiscale approach to CO2 hydrate formation in aqueous solution: phase field theory and molecular dynamics. Nucleation and growth, Journal of Chemical Physics 124 (23) (2006) 234710. doi:10.1063/1.2207138.

[12] S. Becker, H. M. Urbassek, M. Horsch, H. Hasse, Contact angle of sessile drops in Lennard-Jones systems, Langmuir 30 (45) (2014) 13606–13614. doi:10.1021/la503974z.

[13] M. Brinkmann, J. Kierfeld, R. Lipowsky, Stability of liquid channels or filaments in the presence of line tension, Journal of Physics: Condensed Matter 17 (15) (2005) 2349–2364. doi:10.1088/0953-8984/17/15/008.

[14] M. Brinkmann, R. Lipowsky, Wetting morphologies on substrates with striped surface domains, Journal of Applied Physics 92 (8) (2002) 4296–4306. doi:10.1063/1.1506003.

[15] R. Rosso, E. G. Virga, Local stability for a general wetting functional, Journal of Physics A 37 (13) (2004) 3989–4015. doi:10.1088/0305-4470/37/13/006.

[16] P. Blecua, M. Brinkmann, R. Lipowsky, J. Kierfeld, Morphological transitions of liquid droplets on circular surface domains, Langmuir 25 (23) (2009) 13493–13502. doi:10.1021/la901990z.

[17] F. Dorfler, M. Rauscher, S. Dietrich, Stability of thin liquid films and sessile droplets under confinement, Physical Review E 88 (1) (2013) 012402. doi:10.1103/PhysRevE.88.012402.

[18] S. Mechkov, G. Oshanin, M. Rauscher, M. Brinkmann, A. M. Cazabat, S. Dietrich, Contact line stability of ridges and drops, Europhysics Letters 80 (6) (2007) 66002. doi:10.1209/0295-5075/80/66002.

[19] K. Kargupta, R. Konnur, A. Sharma, Instability and Pattern Formation in Thin Liquid Films on Chemically Heterogeneous Substrates, Langmuir 16 (26) (2000) 10243–10253. doi:10.1021/la000759o.

[20] U. Thiele, L. Brusch, M. Bestehorn, M. Bar, Modelling thin-film dewetting on structured substrates and templates: bifurcation analysis and numerical simulations, European Physical Journal E 11 (3) (2003) 255–271. doi:10.1140/epje/i2003-10019-5.

[21] C. Honisch, T.-S. Lin, A. Heuer, U. Thiele, S. V. Gurevich, Instabilities of Layers of Deposited Molecules on Chemically Stripe Patterned Substrates: Ridges versus Drops, Langmuir 31 (38) (2015) 10618–10631. doi:10.1021/acs.langmuir.5b02407.

[22] A. Checco, B. M. Ocko, M. Tasinkevych, S. Dietrich, Stability of thin wetting films on chemically nanostructured surfaces, Physical Review Letters 109 (16) (2012) 166101. doi:10.1103/PhysRevLett.109.166101.

[23] D. Schrade, R. Müller, D. Gross, On the physical interpretation of material parameters in phase field models for ferroelectrics, Archive of Applied Mechanics 83 (10) (2013) 1393–1413. doi:10.1007/s00419-013-0754-5.

[24] P. Yue, C. Zhou, J. J. Feng, Sharp-interface limit of the Cahn–Hilliard model for moving contact lines, Journal of Fluid Mechanics 645 (2010) 279. doi:10.1017/S0022112009992679.

[25] D. N. Sibley, A. Nold, S. Kalliadasis, Unifying binary fluid diffuse-interface models in the sharp-interface limit, Journal of Fluid Mechanics 736 (2013) 5–43. doi:10.1017/jfm.2013.521.

[26] H. Brenner, Interfacial Transport Processes and Rheology, Elsevier Science, Burlington, 1991.
URL http://gbv.eblib.com/patron/FullRecord.aspx?p=1838180

[27] X. Xu, X. Wang, Derivation of the Wenzel and Cassie Equations from a Phase Field Model for Two Phase Flow on Rough Surface, SIAM Journal on Applied Mathematics 70 (8) (2010) 2929–2941. doi:10.1137/090775828.

[28] N. Moelans, B. Blanpain, P. Wollants, An introduction to phase-field modeling of microstructure evolution, Calphad

32 (2) (2008) 268–294. doi:10.1016/j.calphad.2007.11.003.

[29] D. Anders, K. Weinberg, Numerical simulation of diffusion induced phase separation and coarsening in binary alloys, Computational Materials Science 50 (4) (2011) 1359–1364. doi:10.1016/j.commatsci.2010.03.030.

[30] G. N. Wells, E. Kuhl, K. Garikipati, A discontinuous Galerkin method for the Cahn–Hilliard equation, Journal of Computational Physics 218 (2) (2006) 860–877. doi:10.1016/j.jcp.2006.03.010.

[31] A. Rajagopal, P. Fischer, E. Kuhl, P. Steinmann, Natural element analysis of the Cahn–Hilliard phase-field model, Computational Mechanics 46 (3) (2010) 471–493. doi:10.1007/s00466-010-0490-4.

[32] D. Anders, K. Weinberg, A variational approach to the decomposition of unstable viscous fluids and its consistent numerical approximation, ZAMM 91 (8) (2011) 609–629. doi:10.1002/zamm.201000121.

[33] J. W. Cahn, S. M. Allen, A MICROSCOPIC THEORY FOR DOMAIN WALL MOTION AND ITS EXPERIMENTAL VERIFICATION IN Fe-Al ALLOY DOMAIN GROWTH KINETICS, Journal de Physique Colloques 38 (C7) (1977) C7_51–C7_54. doi:10.1051/jphyscol:1977709.

[34] K. M. Schweigler, M. Ben Said, S. Seifritz, M. Selzer, B. Nestler, Experimental and numerical investigation of drop evaporation depending on the shape of the liquid/gas interface, International Journal of Heat and Mass Transfer 105 (2017) 655–663. doi:10.1016/j.ijheatmasstransfer.2016.10.033.

[35] F. Diewald, C. Kuhn, R. Blauwhoff, M. Heier, S. Becker, S. Werth, M. Horsch, H. Hasse, R. Müller, Simulation of Surface Wetting by Droplets Using a Phase Field Model, PAMM 16 (1) (2016) 519–520. doi:10.1002/pamm.201610248.

[36] C. Unger, W. Klein, Nucleation theory near the classical spinodal, Physical Review B 29 (5) (1984) 2698–2708. doi:10.1103/PhysRevB.29.2698.

[37] L. Dong, A. Chaudhury, M. K. Chaudhury, Lateral vibration of a water drop and its motion on a vibrating surface, European Physical Journal E 21 (3) (2006) 231–242. doi:10.1140/epje/i2006-10063-7.